Meson exchange model for $\pi\rho$ scattering

G. Janssen, K. Holinde, and J. Speth
Institut für Kernphysik, Forschungszentrum Jülich GmbH, D-52425 Jülich, Germany
(Received 4 January 1994)

We investigate $\pi\rho$ scattering in the pseudoscalar (π), vector (ω), and axial-vector (A_1) channel using a model based on s- as well as t-channel meson exchange. We start with the realistic case of a broad ρ meson and illustrate the application of three-body methods in this approach. In a second step our calculation is simplified by treating the ρ as a stable particle. Our model is adjusted to reproduce ω- and A_1-resonance parameters and we are able to resolve in a natural way apparent discrepancies occurring in the analysis of the A_1.

PACS number(s): 13.75.Lb, 21.30.+y

I. INTRODUCTION

Although our knowledge about the underlying structure of strong interactions, with quarks and gluons as fundamental degrees of freedom, has increased quite a lot, baryons and mesons have definitely retained their importance as relevant degrees of freedom for a realistic description of low energy nuclear phenomena. The meson-exchange framework has originally been developed to obtain a theoretical understanding of the nucleon-nucleon (NN) interaction. Today there are several potentials based on meson-exchange which are able to describe the NN interaction qualitatively and quantitatively [1]. Having obtained a satisfactory theory of the NN interaction, the meson-exchange framework has been applied to several other processes of medium-energy physics. The concepts of the Bonn potential [2] have, e.g., been extended to meson-baryon and baryon-antibaryon reactions and finally it was possible to describe even meson-meson interactions sucessfully by meson exchange ($\pi\pi$, πK [3]). In this work we continue along this guideline and develop a dynamical model for $\pi\rho$ scattering.

The $\pi\rho$ system is somewhat different from previous examples like NN, πN, or $\pi\pi$ since due to the short lifetime of the ρ meson no $\pi\rho$ scattering data exist which would have to be explained. Therefore, it is not our main aim to investigate elastic $\pi\rho$ scattering but to develop a realistic model for this interaction which can then be applied to the description of other important processes. The main application we have in mind here leads back to the Bonn potential of the NN interaction. There is a long standing discrepancy between the rather hard πNN form factor required by the Bonn potential ($\Lambda_{\pi NN} = 1.3$ GeV) and the strong evidence for a soft form factor deduced from several other sources ($\Lambda_{\pi NN} \simeq 0.8$ GeV) [4]. $\pi\rho$ scattering enters the problem in a twofold way. First, in a meson-exchange model of the πNN form factor one of the dominant diagrams includes a $\pi\rho$ loop and here $\pi\rho$ rescattering can take place [Fig. 1(a)]. It has already been shown that the $\pi\rho$ interaction model we will develop in this work has a strong influence on the πNN form factor leading to an appreciable reduction of the cutoff mass [5] and thus to a soft form factor, in agreement with Ref. [4]. On the other hand, $\pi\rho$ scattering provides an additional contribution which is not yet included in the Bonn potential, namely correlated $\pi\rho$ exchange [Fig. 1(b)]. The results of the present work demonstrate that this diagram can be expected to produce additional tensor force; its inclusion should therefore allow the use of a softer πNN form factor in the Bonn potential and (at least partly) remove this discrepancy.

The large width of the ρ meson does not only prevent $\pi\rho$ scattering experiments, it also complicates the theoretical investigation. Due to the ρ decay the $\pi\rho$ system couples strongly to an underlying 3π system. The description of this coupled channel problem requires the application of three-body methods making the analysis much more complicated. Fortunately, we do not have to solve some relativistic equivalent of the full Faddeev equations [6]. Since the underlying two-body interaction ($\pi\pi \to \rho \to \pi\pi$) is taken to be separable, it is possible to derive an effective two-body scattering equation for $\pi\rho$ scattering. In the present work we apply the relativistic three-body theory of Aaron, Amado, and Young [7] to $\pi\rho$ scattering. However, this calculation leads to an off-shell $\pi\rho$ T matrix which is valid only in a very restricted momentum range. Therefore, and for simplicity reasons, we decided to evaluate a second, simpler model for $\pi\rho$ scattering where the ρ is regarded to be a stable

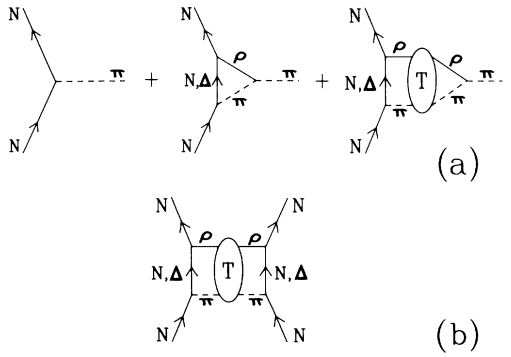

FIG. 1. (a) Meson-exchange model of the πNN form factor. (b) Correlated $\pi\rho$ exchange contribution to the NN potential.

particle. We will compare the results of both models and will show that the main conclusions remain unchanged in the simplified model. Having proven its adequacy this simplified model is then used in all applications where a full off-shell $\pi\rho$ T matrix is required (πNN form factor, correlated $\pi\rho$ exchange).

This work is organized as follows. In the next section we set the theoretical basis of our model. We start by fixing the underlying Lagrangians and derive the general expressions for the pseudopotential V. In the following we discuss in more detail the differences in the potential and scattering equation between a stable ρ model and an unstable ρ model. For the latter we briefly outline the three-body theory of Aaron, Amado, and Young (AAY) [7] and apply it to the $\pi\rho$ system. The last part of the second section contains the treatment of pole diagrams in order to reproduce the properties of the physical particles ω and A_1. In the third section we present our results. After the discussion of the unstable ρ model we show that the simple stable ρ model retains the main physical conclusions. Finally we summarize our results and give an outlook.

II. THE $\pi\rho$ INTERACTION MODEL

A. Determination of the potential V

The starting point of our calculation is the determination of the $\pi\rho$ pseudopotential containing the diagrams which are the relevant ones for the present problem. We take into account s-channel pole diagrams (A_1, ω) as well as exchange diagrams involving the physical π, ρ, and ω (Fig. 2). The pion pole contribution and A_1-exchange terms are not included since they are unimportant, for different reasons: The pion mass lies far below the $\pi\rho$ threshold, and the physical A_1 mass of about 1.2 GeV leads to a very short-ranged contribution only.

Basis for the evaluation of the processes shown in Fig. 2 are the following Lagrangians:

$$\mathcal{L}_{\pi\pi\rho} = g_{\pi\pi\rho}(\boldsymbol{\pi}\times\partial_\mu\boldsymbol{\pi})\cdot\boldsymbol{\rho}^\mu, \tag{1a}$$

$$\mathcal{L}_{\rho\rho\rho} = -\tfrac{1}{2}g_{\rho\rho\rho}(\partial_\mu\boldsymbol{\rho}_\nu - \partial_\nu\boldsymbol{\rho}_\nu)\cdot(\boldsymbol{\rho}^\mu\times\boldsymbol{\rho}^\nu), \tag{1b}$$

$$\mathcal{L}_{A_1\pi\rho} = g_{A_1\pi\rho}\frac{1}{2m_{A_1}}(\partial_\mu\boldsymbol{\rho}_\nu - \partial_\nu\boldsymbol{\rho}_\mu) \cdot[\boldsymbol{\pi}\times(\partial^\mu\mathbf{A}^\nu - \partial^\nu\mathbf{A}^\mu)], \tag{1c}$$

$$\mathcal{L}_{\omega\pi\rho} = g_{\omega\pi\rho}\epsilon^{\mu\nu\sigma\tau}\partial_\mu\omega_\nu\partial_\sigma\boldsymbol{\rho}_\tau\cdot\boldsymbol{\pi}. \tag{1d}$$

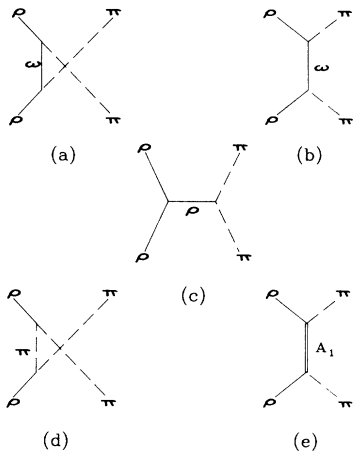

FIG. 2. Diagrams included in the $\pi\rho$ potential.

$\mathcal{L}_{\pi\pi\rho}$ and $\mathcal{L}_{\rho\rho\rho}$ are obtained from models considering the ρ to be the dynamical gauge boson of a hidden local symmetry where the self-coupling of three ρ mesons results from the non-Abelian structure of the underlying gauge group. These models yield for the coupling constant $g \equiv g_{\pi\pi\rho} = g_{\rho\rho\rho} = m_\rho\sqrt{a}/(2f_\pi)$ [8,9]. Taking for a the vector domincance value $a = 2$ we obtain $g^2/4\pi = 2.71$ in remarkably good agreement with results from the decay $\rho\to 2\pi$ leading to $g^2/4\pi = 2.84$. $\mathcal{L}_{\omega\pi\rho}$ and $\mathcal{L}_{A_1\pi\rho}$ may be regarded as extensions of this gauge particle approach to A_1 and ω mesons [9] and similar relations could be obtained for the couplings. However, the $A_1\pi\rho$ coupling appears in a pole diagram only and here as well as for the ω pole diagram we have to use bare coupling constants $g^{(0)}$ since the coupling is renormalized by the iteration in a scattering equation which will be discussed below. Together with the bare masses $m^{(0)}$ they are adjusted to reproduce the resonance parameters of A_1 and ω (Sec. II D). The coupling constant $g_{\omega\pi\rho}$ appearing in the ω exchange diagram is obtained from a study of the decay $\omega\to\pi\rho\to\pi\gamma$ to become $(g^2_{\omega\pi\rho}/4\pi)\,m^2_\omega \simeq 7.5$ [10].

The calculation of the Feynman diagrams contributing to V (Fig. 2) using the Lagrangians of Eqs. (1) follows standard lines; therefore we restrict ourselves to the presentation of the result (a dot indicates a product between four-vectors):

(a) $\boldsymbol{\pi}$ exchange

$$V = -g^2\,I\,F^2 d(2q-k')\cdot\epsilon^*(2q'-k)\cdot\epsilon. \tag{2a}$$

(b) $\boldsymbol{\omega}$ exchange

$$V = g^2_{\omega\pi\rho}\,I\,F^2\,d\{q\cdot q'[k\cdot k'\epsilon\cdot\epsilon^* - k'\cdot\epsilon\,k\cdot\epsilon^*] + q\cdot k[k'\cdot\epsilon q'\cdot\epsilon^* - q'\cdot k'\epsilon\cdot\epsilon^*] + q\cdot\epsilon[q'\cdot k'k\cdot\epsilon^* - k\cdot k'q'\cdot\epsilon^*]\}. \tag{2b}$$

(c) $\boldsymbol{\rho}$ exchange

$$V = g^2IF^2d\{(q+q')\cdot\epsilon[2k\cdot\epsilon^* - k'\cdot\epsilon^*] + (q+q')\cdot\epsilon^*[2k'\cdot\epsilon - k\cdot\epsilon] - \epsilon\cdot\epsilon^*(q+q')\cdot(k+k')\}. \tag{2c}$$

(d) ω pole

$$V = (g^{(0)}_{\omega\pi\rho})^2\, I\, F^2\, d^{(0)}\; s\{[k\cdot k'\epsilon\cdot\epsilon^* - k'\cdot\epsilon k\cdot\epsilon^*] + k_0[\epsilon_0^* k'\cdot\epsilon - k'_0\epsilon\cdot\epsilon^*] + \epsilon_0[k'_0 k\cdot\epsilon^* - \epsilon_0^* k\cdot k']\}. \tag{2d}$$

(e) A_1 pole

$$V = (g^{(0)}_{A_1\pi\rho})^2/m^2_{A_1}\, I\, F^2\, d^{(0)}\; s\{k'_0[\epsilon_0 k\cdot\epsilon^* - k_0\epsilon\cdot\epsilon^*] + \epsilon_0^*[k_0\; k'\cdot\epsilon - \epsilon_0 k\cdot k']\}. \tag{2e}$$

In order to ensure convergence of the scattering equation (to be applied later) we have added phenomenological form factors of standard monopole or dipole type for each vertex, the product is abbreviated by F^2 in Eqs. (2). ϵ and ϵ^* denote the polarization vectors for an incoming and outgoing ρ meson (Fig. 3), respectively, the Mandelstam variable s is defined by $s = E^2_{\rm cms}$ and the isospin factor I for each diagram is given in Table I. The propagator d for the exchanged particle ($d^{(0)}$ for pole diagrams) depends on the model we use for the iteration of the pseudopotential. Its explicit form will be determined below.

B. Three-particle case (unstable rho)

Having obtained the expressions for the pseudopotential V we have to specify a model for the iteration of this potential in a scattering series to obtain the full scattering amplitude. This will be done first for the more realistic case of a broad ρ. In the next section certain approximations will be performed yielding a simpler model including a stable ρ meson.

1. The basic formalism

Since the rather large width of the ρ meson (150 MeV) is generated by the decay $\rho \to 2\pi$, the $\pi\rho$ system which we investigate couples strongly to the 3π system. Therefore a rigorous treatment requires in principle the application of three-body methods. In the following we briefly report the relativistic three-body theory of Aaron, Amado, and Young (AAY) [7] and apply it to the $\pi\rho$ system.

As it is known for the nonrelativistic three-body problem the full set of Faddeev equations [6] can be reduced to an effective two-body Lippmann-Schwinger equation under the assumption that the underlying two-body interaction is separable or, in other words, if the two-body interaction proceeds via an isobar. This concept can be generalized to the relativistic case and leads to an effective two-body Bethe-Salpeter equation as the starting point of the AAY calculation

$$T(s;q',q) = V(s;q',q) + (2\pi)^{-4}\int d^4p\; V(s;q',p)\mathcal{D}(\sigma_p)T(s;p,q)\;, \tag{3}$$

where q, q', and p are pion momenta, $s = P^2$ denotes the square of the total four-momentum, and $\sigma_p = (P-p)^2$ denotes the square of the four-momentum of the intermediate ρ subsystem (Fig. 4).

In order to get a soluable (three dimensional) scattering equation further simplifications are necessary. As in the two-body case one tries to find a form of $\mathcal{D}$ which, on the one hand, reduces the dimensionality of Eq. (3) but, on the other hand, does not influence the unitarity of the scattering amplitude T.

Assuming only two- and three-body intermediate states the unitarity requirement is given by

$$T_{fi} - T^\dagger_{fi} = -i\sum_n d\Omega_n\, T_{fn}T^\dagger_{ni} = -i\int d\Omega_2\, T_{22}T^\dagger_{22} - i\int d\Omega_3 T_{23}T^\dagger_{32} \tag{4}$$

with

$$d\Omega_n = (2\pi)^4\delta^4\left(P - \sum_{i=1}^n q_i\right)\prod_{i=1}^n \frac{d^4q_i}{(2\pi)^4}\,2\pi\delta^+(q_i^2 - m_i^2)\;. \tag{5}$$

In the AAY calculation a second expression for $T - T^+$ is derived from the Bethe-Salpeter equation yielding

$$T - T^+ = [V - V^+] + T^+\mathcal{D}^+[V - V^+] + [V - V^+]\mathcal{D}T + T^+[\mathcal{D} - \mathcal{D}^+]T + T^+\mathcal{D}^+[V - V^+]\mathcal{D}T\;, \tag{6}$$

where $T \equiv T(s + i\epsilon)$ and $T^+ \equiv T^\dagger(s + i\epsilon) = T(s - i\epsilon)$ ($\mathcal{D}$ and V analogous).

Taking matrix elements in momentum space it is obvious that for

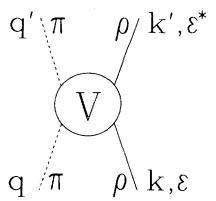

FIG. 3. Diagram defining incoming and outgoing particles.

TABLE I. Isospin factors for the different diagrams.

Diagram	$T=0$	$T=1$	$T=2$
π exchange	+2	−1	−1
ρ exchange	+2	+1	−1
ω exchange	+1	−1	+1
A_1 pole	0	+2	0
ω pole	+3	0	0

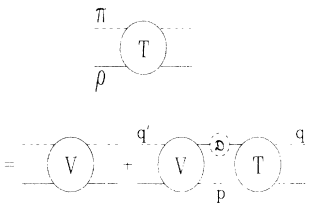

FIG. 4. The effective two-body Bethe-Salpeter equation.

$$\text{disc}[V(p,q)] = 0,\ \text{disc}[V(q',p)] = 0\ \forall p \quad \text{and } \text{disc}[V(q',q)] = 0 \tag{7}$$

the first three terms on the right hand side of Eq. (6) vanish. Following the AAY calculation we postpone the discussion of the restrictions due to Eq. (7) for the moment and compare the resulting equation

$$\begin{aligned}\text{disc}[T] &\equiv T - T^+ \\ &= T(\mathcal{D} - \mathcal{D}^+)T^+ + T\mathcal{D}(V - V^+)\mathcal{D}T^+ \end{aligned} \tag{8}$$

with Eq. (4). Evaluating the latter explicitly expressions for disc$[V]$ and disc$[\mathcal{D}]$ can be determined from this comparison.

Having obtained the discontinuities of $\mathcal{D}$ and V one can deduce an explicit expression for these quantities, which is of course by no means unique. For details of this calculation the reader is referred to [7]. We report the results here (modified for the present problem of $\pi\rho$ scattering) to define the ingredients of our model.

The potential V arising from pion exchange has the following form (isospin neglected)

$$V_\pi(s;\mathbf{q}',\mathbf{q}) = -f_1 \overbrace{\frac{\omega_q + \omega_{q'} + \omega_x}{\omega_x[s - (\omega_q + \omega_{q'} + \omega_x)^2]}}^{d} f_2 \tag{9}$$

with

$$\omega_x = \sqrt{q^2 + q'^2 + m_\pi^2 + 2qq'\cos\theta}\ . \tag{10}$$

f_1 and f_2 are the $\pi\pi\rho$ vertex functions appearing in Eq. (2a) with the modification that the dispersion integral performed by AAY to obtain V_π from disc$[V_\pi]$ forces $\sqrt{s}$ to $\sqrt{s} = \omega_q + \omega_{q'} + \omega_x$:

$$\begin{aligned} &g\,(2q - k')\cdot\epsilon^* = g\,[2q - (\sqrt{s},\mathbf{0}) + \mathbf{q}']\cdot\epsilon^* \\ &\quad\to\ [2q + q' - (\omega_q + \omega_{q'} + \omega_x,\mathbf{0})]\cdot\epsilon^* \equiv f_1 \\ &g\,(2q' - k)\cdot\epsilon\ = g\,[2q' - (\sqrt{s},\mathbf{0}) + \mathbf{q}]\cdot\epsilon \\ &\quad\to\ [2q' + q - (\omega_q + \omega_{q'} + \omega_x,\mathbf{0})]\cdot\epsilon\ \equiv f_2\ . \end{aligned} \tag{11}$$

The propagator $\mathcal{D}$ in the Bethe-Salpeter equation is given by

$$\mathcal{D}(\sigma_p) = 2\pi\delta^+(p^2 - m_\pi^2)D(\sigma_p)\ . \tag{12}$$

This δ function reduces the dimensionality of the scattering equation and puts the spectator pion on-mass shell. Furthermore, since $p^2 = m_\pi^2$,

$$\sigma_p = (P - p)^2 = s - 2\sqrt{s}\,\omega_p + m_\pi^2\ . \tag{13}$$

$D(\sigma_p)$ denotes the propagator of the intermediate ρ subsystem in the three-dimensional scattering equation

$$\begin{aligned} D(\sigma_p) &= \left[(2\pi)^3 2\omega_p\right]^{-1} \\ &\times\left[\sigma_p - (m_\rho^{(0)})^2 - \int \frac{d^3p'}{(2\pi)^3\omega_{p'}} \frac{(f_{\pi\pi\rho}^{(0)})^2}{(\sigma_p - 4\omega_{p'}^2)}\right]^{-1}, \end{aligned} \tag{14}$$

and is determined such that it reproduces the main features of the two-body $(\pi\pi)$ subsystem (see below).

It is clear that further diagrams with disc$[V] = 0$ can be included in V. In our calculation the potential V contains in addition to the pion exchange [Eq. (9)] ρ and ω exchange as well as the pole diagrams. The propagator d for these diagrams is taken to be the usual Feynman propagator $d = [K_x^2 - m_x^2]^{-1}$ where K_x denotes the four-momentum and m_x the mass of the exchanged particle. Since the spectator pion is kept on-mass shell, four-momentum conservation fixes the four-momenta of the involved ρ mesons: $k_0 = \sqrt{s} - \omega_q$, $k_0' = \sqrt{s} - \omega_q'$.

We finally get a three-dimensional effective two-body scattering equation

$$\begin{aligned} T(s;q',q) &= V(s;q',q) \\ &+ \int \frac{d^3p}{(2\pi)^3 2\omega_p} V(s;q',p)D(\sigma_p)T(s;p,q)\ . \end{aligned} \tag{15}$$

2. *Application to the $\pi\rho$ system*

The fundamental ingredient of the three-body theory developed in the last section was the assumption of an underlying separable two-body $(\pi\pi)$ interaction. In terms of a meson exchange model this implies that the vector/isovector part of the $\pi\pi$ T matrix is generated exclusively by a ρ pole diagram and thus can be written as (cf. Subsec. D)

$$\begin{aligned} &T_{\pi\pi}^{J,T=1}(s_{\pi\pi};q',q) \\ &= f_{\pi\pi\rho}^{(0)}(s_{\pi\pi};q')\frac{1}{s_{\pi\pi} - (m_\rho^{(0)})^2 - \Sigma(s_{\pi\pi})} f_{\pi\pi\rho}^{(0)}(s_{\pi\pi};q) \\ &= f_{\pi\pi\rho}^{(0)}\,\tilde{d}\,f_{\pi\pi\rho}^{(0)} \end{aligned} \tag{16}$$

with

$$\Sigma(s_{\pi\pi}) = \int d^3p' \frac{1}{(2\pi)^3\omega_{p'}} \frac{(f_{\pi\pi\rho}^{(0)})^2}{s_{\pi\pi} - 4\omega_{p'}^2}\ . \tag{17}$$

Once we have fixed the parameters $g^{(0)}$ (implicitly contained in $f_{\pi\pi\rho}^{(0)}$ and therefore also in Σ) and $m^{(0)}$ to reproduce the $\pi\pi$ vector or isovector phases we have at the same time determined the propagator $D(\sigma_p)$. It is obvious that $D(\sigma_p)$ is obtained from $\tilde{d}(s_{\pi\pi})$ by the replacement $s_{\pi\pi} \to \sigma_p$, i.e., by the inclusion of the spectator pion. Figure 5 shows a comparison of $D(\sigma_p)$ with the two-body propagator G of Subsec. C demonstrating the transition from a zero-width ρ meson to a broad one.

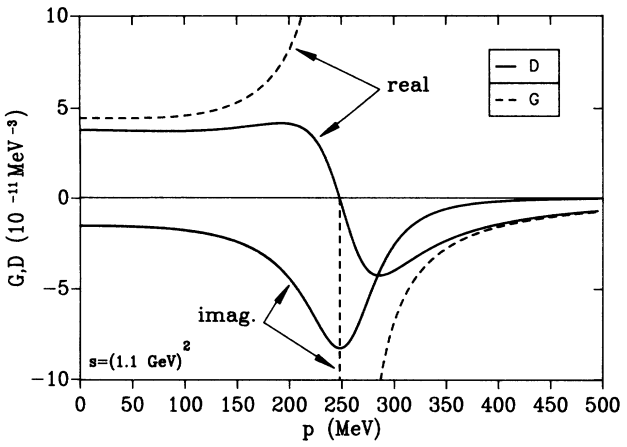

FIG. 5. Comparison of the propagator G of a stable $\pi\rho$ system and the propagator D of a 3π system.

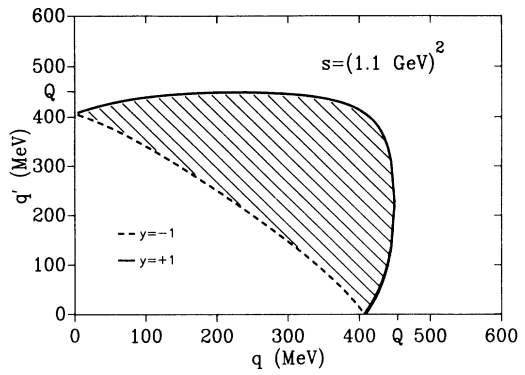

FIG. 6. Singularities of the pion exchange potential V_π^J. V_π^J is complex for all combinations of q and q' inside the shaded area. Solutions for $\sqrt{s}-\omega_q-\omega_{q'}-\omega_x(y=\pm1)=0$ are shown [Eq. (19)].

To solve the scattering equation (15) we have to perform the momentum integration along the real axis. The singularities of the propagator $D(\sigma_p)$ are positioned in the complex plane far away from the real axis and thus do not have any influence on this integration. The situation appears to be more complicated for the pion exchange part of the potential V, which may be written in a partial wave decomposed form

$$V_\pi^J(s;q',q) = \int_{-1}^{+1} dy \frac{\tilde{V}_\pi(s;q',q;y)}{\sqrt{s}-\omega_q-\omega_{q'}-\omega_x(q,q';y)} \qquad y := \cos(\theta) \ . \tag{18}$$

For certain values of s, q, and q' the integrand may become singular and the integration leads to a complex potential V_π^J. After regularizing this integration the real part of V_π^J contains moving logarithmic singularities

$$V_\pi^J(s;q',q) \sim \ln\left|\frac{\sqrt{s}-\omega_q-\omega_{q'}-\omega_x(y=-1)}{\sqrt{s}-\omega_q-\omega_{q'}-\omega_x(y=+1)}\right| \ . \tag{19}$$

Figure 6 shows the position of these singularities in the (q,q') plane. For (q,q') lying in the shaded area between the singularity curves the potential V_π^J is complex, i.e., $\mathrm{disc}(V_\pi^J)\neq 0$. Outside this area the propagator in Eq. (18) cannot become singular and thus V_π^J remains real.

At this point it is necessary to continue the discussion of the validity of Eq. (8). It was discussed above that this equation only holds if $\mathrm{disc}[V(p,q)] = 0\ \forall p$, $\mathrm{disc}[V(q',p)] = 0\ \forall p$, and $\mathrm{disc}[V(q',q)] = 0$. Figure 6 immediately shows that this is fulfilled only for $q,q' > Q$. Q is s dependent and given by

$$Q = \sqrt{\left(\frac{s-3m_\pi^2}{2\sqrt{s}}\right)^2 - m_\pi^2} \ . \tag{20}$$

In summary, the present approach to the three-body system allows the calculation of $T(s;q',q)$ only for $q,q' > Q$ (this may be seen as an advantage since we then have no problems with the moving singularities of V_π^J while solving the scattering equation). Fortunately, it turns out (Sec. III) that this is sufficient for the calculation of mass distributions, i.e., for our investigations in the A_1 and ω channel. However, in the calculation of the πNN form factor [5] or of correlated $\pi\rho$ exchange between two nucleons, a full off-shell $\pi\rho$ T matrix is required. Therefore, we present in the next chapter a simplified model neglecting the width of the ρ meson, which is able to provide a full off-shell $\pi\rho$ T matrix.

C. Two-particle case (stable rho)

Treating the ρ meson as a stable particle we can apply the usual two-body formalism to obtain the scattering amplitude T from the pseudopotential V. Equation (3) is then replaced by the well-known two-body Bethe-Salpeter equation

$$T = V + \int d^4p\, V\mathcal{G}(s)T \ , \tag{21}$$

where p denotes the relative momentum of the $\pi\rho$ system. Again, the dimensionality of this equation can be reduced by making a certain choice for the propagator $\mathcal{G}$ with the constraint that T remains unitary. In our calculation we use the Blankenbecler-Sugar scheme for this reduction [11] with a slightly modified propagator $\mathcal{G}$ introduced for instance by Aaron [7]

$$\mathcal{G}(p,s) = \delta\left(p_0-\frac{1}{2}\omega_\pi+\frac{1}{2}\omega_\rho\right)\frac{\pi}{\omega_\pi\omega_\rho}\frac{\omega_\pi+\omega_\rho}{s-(\omega_\pi+\omega_\rho)^2} =: 2\pi\delta\left(p_0-\frac{1}{2}\omega_\pi+\frac{1}{2}\omega_\rho\right)(2\pi)^3\,G(\mathbf{p},s) \tag{22}$$

with $\omega_\alpha = \sqrt{\mathbf{p}^2+m_\alpha^2}$. The δ function in front of $\mathcal{G}$ reduces the dimensionality of the scattering equation and determines the off-shell behavior of the potential V.

The propagator d (or d_0) for each exchanged particle in the pseudopotential diagrams has the form

$$d = [K_x^2 - m_x^2]^{-1} \ , \tag{23}$$

where K_x denotes the four-momentum and m_x the mass of the exchanged particle (for pole diagrams $m_x^{(0)}$ is used).

When the pion exchange contribution to V is calculated using this form of d and the off-shell behavior defined by Eq. (22) problems arise since it turns out that the propagator d creates unphysical singularities. The reason for this lies in the fact that the pion exchange diagram contains the propagation of three pions (Fig. 7), a process which above 3π threshold cannot properly be described by the simple form of d given in Eq. (23). It is obvious that a physically satisfactory form for the pion exchange propagator can only be found in the three-body formalism as it was done in the last section; however, in order to create a simple model (stable ρ meson, i.e., no three-body effects) we decided to use the static propagator approximation for d

$$d = [\mathbf{K}_\pi^2 - m_\pi^2]^{-1} = -\omega_x^{-2} , \tag{24}$$

thus eliminating any singularities.

Having obtained the potential V and fixed the form of the scattering equation we can proceed using standard methods. After partial-wave decomposition and transformation into the LSJ basis the remaining one-dimensional integral equation is solved by matrix inversion, yielding the T matrix for $\pi\rho$ scattering.

D. Pole diagrams, determination of poles

There are three states of the $\pi\rho$ system that are characterized by quantum numbers identical to those of important physical particles

$$\begin{aligned} L_{JT} &= P_{01} \leftrightarrow \pi - \text{meson}, \\ L_{JT} &= P_{10} \leftrightarrow \omega - \text{meson}, \\ L_{JT} &= S_{11} \leftrightarrow A_1 - \text{meson}. \end{aligned}$$

In the following we discuss the inclusion of these particles in our model in order to evaluate a $\pi\rho$ amplitude that reflects our experimental knowledge about π, ω, and A_1. We would like to note here that due to selection rules a contribution to the NN potential from correlated $\pi\rho$ exchange is obtained only if the exchanged $\pi\rho$ system exists in one of the states mentioned above (exept for unimportant higher J contributions). A correct treatment of these channels is therefore quite important.

1. π-meson channel

As was already mentioned the π-meson mass lies far below $\pi\rho$ threshold and even below 3π threshold. The pion has therefore a negligibly small effect on elastic $\pi\rho$ scattering and we do not have to include anything like a pion pole diagram in our model.

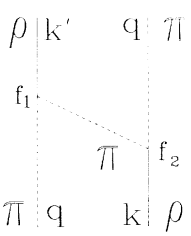

FIG. 7. A time-ordered contribution to the pion exchange diagram.

2. ω-meson channel

Since the ω-meson mass lies above 3π threshold, but below $\pi\rho$ threshold, the treatment of this particle depends on the model we use for the $\pi\rho$ system. For an unstable ρ (i.e., if we investigate a 3π system) the ω meson appears to be a "normal" resonance of three pions having a certain mass and width (although the latter is quite small, $\Gamma_\omega \simeq 8$ MeV). If we consider the ρ to be stable (with a mass of 769 MeV), the ω meson can no longer decay into π and ρ being a zero-width particle in this model. Nevertheless, since the ω lies rather close to $\pi\rho$ threshold, it definitely has an influence on the $\pi\rho$ amplitude so that an ω pole diagram should be included for a stable as well as for an unstable ρ meson.

a. ω-meson for the stable ρ model. After partial wave decomposition the potential in the ω channel can be divided into a pole and a nonpole part

$$V_{P_{10}} = V_{P_{10}}^{p} + V_{P_{10}}^{np}, \tag{25}$$

where the pole part consists of the ω pole diagram only, whereas the nonpole part contains π, ω, and ρ exchange. Iterating this potential in a scattering equation $T = V + VGT$ (suppressing the L_{JT} index), it can be shown [12] that the T matrix also separates into a pole and a nonpole part:

$$T = T^{\mathrm{np}} + T^{p} = T^{\mathrm{np}} + f\,\tilde{d}\,f, \tag{26a}$$

$$T^{\mathrm{np}} = V^{\mathrm{np}} + V^{\mathrm{np}} G T^{\mathrm{np}}, \tag{26b}$$

$$f = f^{(0)} + f^{(0)}\,G\,T^{\mathrm{np}}, \tag{26c}$$

$$\tilde{d} = (d^{(0)} - \Sigma)^{-1}, \tag{26d}$$

$$\Sigma = f^{(0)} G f, \tag{26e}$$

where $f^{(0)}$ denotes the bare $\omega \to \pi\rho$ vertex function in a partial wave decomposed form and can be written as

$$f^{(0)}(s,q) = \sqrt{[(g^{(0)} m_\omega)^2/4\pi]\, 32\,\pi^2\, s m_\omega^{-2}}\; q\, F(q) \ . \tag{27}$$

$f^{(0)}$ and therefore also f and Σ contain the bare coupling constant $g^{(0)}$, the propagator $d^{(0)}$ contains the bare mass $m^{(0)}$. The self-energy $\Sigma(s)$ is real at $s = m_\omega^2$ indicating that the ω meson is a zero-width particle in this approach. The requirement of a pole of T^p at the physical ω mass therefore fixes only one of the two parameters, namely $m^{(0)}$,

$$d^{(0)}(m_\omega^2) - \Sigma(m_\omega^2) = m_\omega^2 - (m^{(0)})^2 - \Sigma(m_\omega^2) \stackrel{!}{=} 0 \ . \tag{28}$$

The bare coupling constant $g^{(0)}$ [included in Σ in Eq. (26e)] has to be determined using the independent condition that T^p has the right residue at the ω pole which

includes the physical coupling constant g. One obtains [12]

$$(g^{(0)})^2 = g^2 \left[\frac{\tilde{f}^2}{(\tilde{f}^{(0)})^2} + g^2 \frac{\partial}{\partial s} \tilde{\Sigma}(s) \right]^{-1} \quad (29)$$

with $f =: g^{(0)}\tilde{f}, f^{(0)} =: g^{(0)}\tilde{f}^{(0)}$ and $\Sigma =: (g^{(0)})^2\tilde{\Sigma}$.

b. ω meson for the unstable ρ model. Using the unstable ρ model the underlying algebra leading to Eqs. (26) remains in principle unchanged with G replaced by the three-pion propagator D. (It was shown in Subsec. B that the unstable ρ model does not allow the calculation of a fully off-shell T matrix. From this point of view $T_{\rm np}$ is not well defined fully off-shell since it is not a unitary amplitude for all momenta. However, we can just *define* a certain function $T^{\rm np}$ by Eq. (26b) and this expression can then be used to determine the self-energy Σ. Alternatively, we could have calculated Σ by using, e.g., the equation $T(s;q,q) = T^{\rm np}(s;q,q) + f(s;q)[s - (m^{(0)})^2 - \Sigma(s)]^{-1} f(s;q)$, where q is an arbitrary momentum larger than Q [Eq. (20)] and hence all involved functions (T, $T^{\rm np}$, f) are physically well defined).

The really important difference in comparison to the stable ρ model lies in the fact that the self-energy $\Sigma = f^{(0)}Df$ is now complex for all values of s larger than $(3m_\pi)^2$ and the ω meson has therefore a certain width in this model. If we compare

$$\left[s - \left(m_\omega - i\frac{\Gamma_\omega}{2} \right)^2 \right]^{-1} \simeq \left[s - m_\omega^2 + i m_\omega \Gamma_\omega \right]^{-1} \quad (30)$$

with

$$\left[s - (m^{(0)})^2 - \Sigma(s) \right]^{-1}, \quad (31)$$

we get two equations to determine $g^{(0)}$ and $m^{(0)}$

$$\begin{aligned} m_\omega^2 &= (m^{(0)})^2 + \mathrm{Re}\ \Sigma((m_\omega - i\Gamma_\omega/2)^2), \\ -\Gamma_\omega m_\omega &= \mathrm{Im}\Sigma((m_\omega - i\Gamma_\omega/2)^2) \ . \end{aligned} \quad (32)$$

3. A_1-meson channel

The A_1 meson has a mass around 1260 MeV (details are discussed in Sec. III) and lies above 3π threshold as well as above $\pi\rho$ threshold. For both models (stable unstable ρ) we have to apply the formalism explained in 2. b) for the ω meson resulting in Eqs. (32). The corresponding bare vertex function is given by

$$\begin{aligned} f^{(0)}(s,q) &= \frac{g^{(0)}}{\sqrt{4\pi}} \frac{4\pi\sqrt{s}F(q)}{3m_\rho} \\ &\times \left(2k_0 + \frac{k_o \omega_\rho(q) - q^2}{m_\rho} \right), \end{aligned} \quad (33)$$

where k_0 denotes the zeroth component of the ρ four-momentum, which depends on the off-shell structure we use.

To determine the pole of the $\pi\rho$ scattering amplitude the self-energy $\Sigma(s)$ has to be determined for complex values of s. Details of this calculation are given in Appendix A.

III. RESULTS

In the last section we have developed two interaction models for $\pi\rho$ scattering, one assuming the ρ to be a stable particle (model B in the following), the other including the decay width of the ρ meson (model A). In this section we will present the results we obtain using these models of the $\pi\rho$ T matrix.

Before we start we would like to make a short remark about the ingredients of our pseudopotential, in particular about the role of ω exchange. Figure 8 shows the on-shell potentials for model B in the three partial waves of interest when only exchange (nonpole) diagrams are included. Obviously ρ exchange provides the dominant contribution in the A_1 partial wave whereas in P waves π exchange is of comparable strength. Figure 8 further demonstrates that ω exchange is quite unimportant in all partial waves. For model A ω exchange is somewhat problematic since for the off-shell structure used in this case the ω propagator creates unphysical singularities. We avoid these problems by assuming that ω exchange is as unimportant for model A as it is for model B and neglect this contribution in both models.

We start our analysis by investigating the A_1 (S_{11}) channel. Empirically our knowledge about the A_1 meson is based on two different classes of experiments [13]. The first class contains investigations of the leptonic decay $\tau \to \nu_\tau A_1 \to \nu_\tau 3\pi$ which proceeds via an intermediate virtual W boson [Fig. 9(a)]. The corresponding experiments are expected to be free from any background so that the extracted A_1 parameters are reliable. For the present analysis we make use of the working hypothesis that the results derived from τ decay are the correct ones, i.e., we assume

$$m_{A_1} \simeq 1260\ \mathrm{MeV}, \quad \Gamma_{A_1} \simeq 400\ \mathrm{MeV}\ [13,14]. \quad (34)$$

The second class of experiments investigates hadronically produced A_1 mesons. It may be subdivided into diffractive production ([13], $\pi p \to 3\pi p$) and charge-exchange production ([15], $\pi p \to 3\pi n$). In both cases the analysis is troubled by the existence of a significant background and it is one aim of this work to get a theoretical understanding of this background. We will do this for the charge-exchange reaction since this reaction proceeds via the exchange of a ρ meson and allows a direct application of our $\pi\rho$ interaction model [Fig. 9 (b)]. Charge-exchange data from Ref. [15] are given in some of the following figures. From these results and without the inclusion of any background the authors derive an A_1 mass of 1.13 GeV (unfortunately no width) in apparent disagreement with the τ-decay results. (In addition, they introduce a certain phenomenological background to remove this discrepancy.)

Our theoretical model can clarify this situation since it allows us to determine both the experimentally observed

mass spectrum and the pole parameters of the A_1. The former is given by

$$\sigma(t, M_{3\pi}) = f(t)\,\sigma_{\pi\rho}(t, M_{3\pi}) \tag{35}$$

where $M_{3\pi}$ denotes the invariant 3π mass, $\sigma_{\pi\rho}$ is the mass spectrum for the reaction $\pi\rho \to 3\pi$, and $f(t)$ is a function containing the $NN\rho$ vertex, the ρ propagator, and so on. $\sigma_{\pi\rho}$ is given by [16]

$$\sigma_{\pi\rho}(t, M_{3\pi}) = \int d\Omega_3\, T_{23} T_{32}^{\dagger} = -2\,\mathrm{Im}[T_{\pi\rho}(t, M_{3\pi})] \ . \tag{36}$$

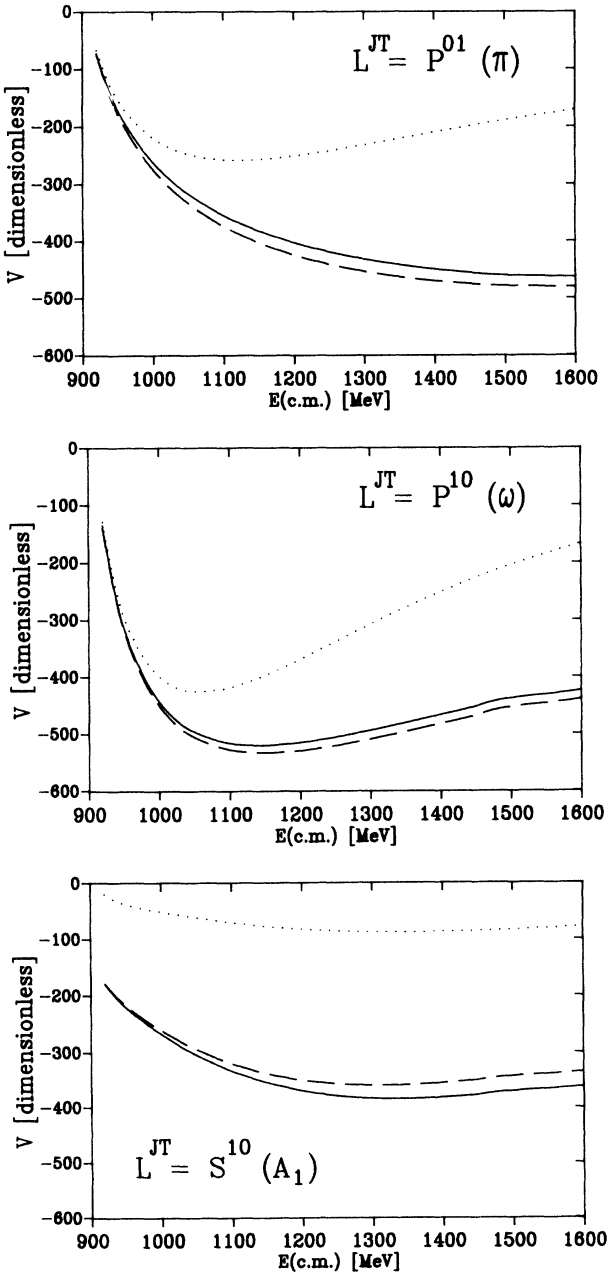

FIG. 8. On-shell potentials in π-, ω-, and A_1-partial waves arising from nonpole diagrams in model B. The dotted line contains only π exchange; for the solid line ρ exchange is added. The dashed line includes all exchange diagrams.

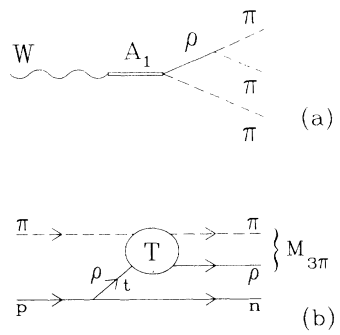

FIG. 9. Reactions including the A_1 meson. (a) The dominant diagram contributing to $\tau \to \nu 3\pi$ decay. (b) Charge-exchange reaction $\pi p \to 3\pi n$. t denotes the four-momentum squared of the exchanged ρ meson.

Here, $T_{\pi\rho}$ denotes the off-shell T matrix for $\pi\rho$ scattering that was calculated in Sec. II using model A. It is an advantage of this model that the off-shell structure forces the pion to be on-mass shell whereas the ρ meson can be off-shell. This is exactly the situation we find in the charge-exchange experiment [Fig. 9 (b)] and $T_{\pi\rho}(t, M_{3\pi})$ can therefore be written in the more common form

$$T_{\pi\rho}(s = M_{3\pi}^2; k, k) \quad \text{with } k = \sqrt{\left[\frac{s + m_\pi^2 + t}{2\sqrt{s}}\right]^2 - m_\pi^2} \ . \tag{37}$$

In the experiment t is always lower than zero; Fig. 10 shows the k value corresponding to $t = 0$ which depends on s. This figure shows in addition the value Q that bounded the region where the π-exchange potential is complex. As was discussed in Sec. II B the three-body theory can only be applied for momenta larger than Q and Fig. 10 shows that in the present case this is fulfilled for all values of $M_{3\pi}$ and all $t < 0$.

As will be discussed below in Fig. 14 the t dependence

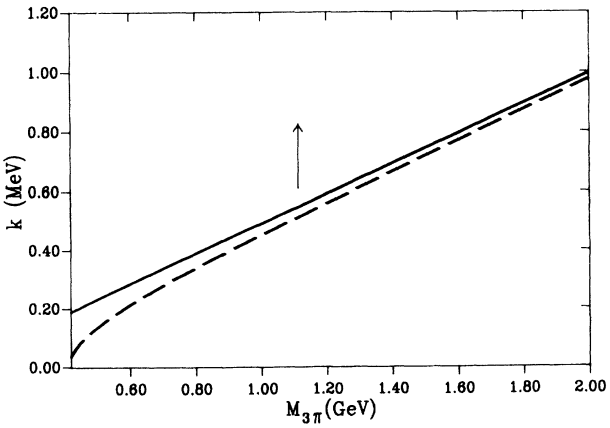

FIG. 10. The solid line shows the ρ momentum k corresponding to $t = 0$ as a function of $M_{3\pi}$. The dashed line shows the boundary Q for disc$[B] \neq 0$. The arrow indicates the movement of the solid curve when t is varied ($t < 0$).

of the shape of the mass spectrum is rather weak. We therefore make use of the approximation

$$\sigma(t, M_{3\pi}) = \tilde{f}(t)\, \sigma_{\pi\rho}(t=0, M_{3\pi}) \tag{38}$$

and $\sigma_{\pi\rho}(t=0, M_{\pi\rho}) \equiv \sigma$ will be compared with experimental data.

To get a feeling for the importance of the different contributions to the potential we first calculate the mass spectrum using exclusively the A_1-pole diagram and do not include any exchange contribution. As described in Sec. II D we fix the pole at the A_1 mass [Eq. (34)] and vary the only remaining parameter, the cutoff mass appearing in the form factor $F(q)$ in Eq. (33). In all model A calculations that follow we have looked for the pole on the second as well as on the third sheet. We have never been able to find an A_1 pole on the second sheet but always on the third one. Results (normalized to experimental data) are shown in Fig. 11. Obviously it is not possible to describe the experimental data by including only the A_1-pole diagram. On the other hand, it is definitely not possible to renounce this diagram and generate the experimentally observed bump by iterating the exchange part of the potential only. This is demonstrated in Fig. 12, which shows the mass spectrum resulting from the nonpole part $T_{\rm np}$ only. We have chosen arbitrary cutoff masses for π- and ρ exchange but the result turns out to be rather independent of this choice. Figure 12 also demonstrates that ρ exchange provides the dominant contribution to the nonpole part of the mass spectrum. This is qualitatively understandable since we found out that for π exchange the Born approximation works quite well. Therefore $\sigma_{\pi-\rm ex} \sim \mathrm{Im}\, T_{\pi-\rm ex} \simeq \mathrm{Im}\, V_{\pi-\rm ex} = 0$.

Both parts on their own, exchange diagrams and the A_1-pole diagram, are not sufficient for an understanding of the experimental data. However, if we put these parts together, the situation changes. Note that $T_{\rm np}$ influences the mass spectrum in two ways; first it implicitly changes

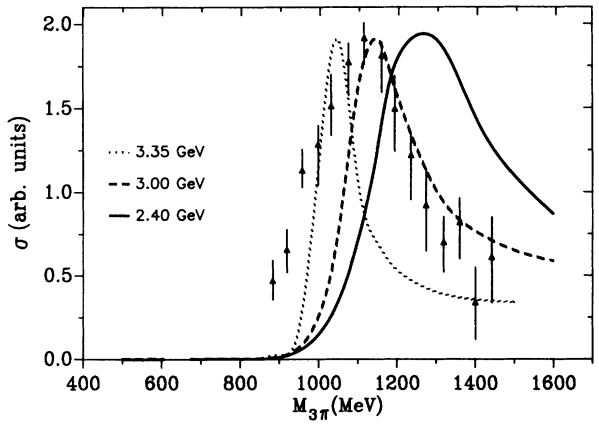

FIG. 11. The mass spectrum in the A_1 channel. The figure shows the data of Ref. [15]. In addition, it contains the model A result for the mass spectrum when no exchange diagrams are included in the potential. The different curves are obtained for different values of the cutoff mass appearing in the $A_1 \to \pi\rho$ vertex function. The pole is fixed at $1260 - i\,400/2$ MeV.

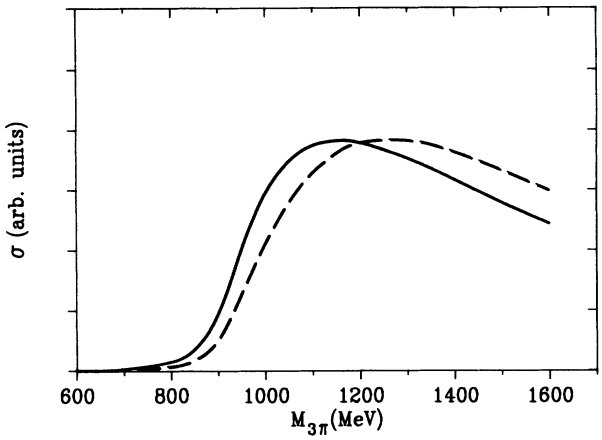

FIG. 12. The mass spectrum in the A_1 channel of the $\pi\rho$ system (without any A_1 pole). The dashed line shows the result when only ρ exchange is included in the potential. The solid line contains in addition π exchange.

the pole part from $f^{(0)}\tilde{d}f^{(0)}$ to $f\tilde{d}f$, second it is added to the pole-part T_p to yield the total T matrix [Eq. (26a)]. The result is shown in Fig. 13. Again the pole of T is fixed to reproduce the A_1 parameters of Eq. (34). But in contrast to Fig. 11 it is now possible to get agreement with the experimental data.

In summary, we are able to describe the experimental charge-exchange data and, at the same time, find an A_1 mass in agreement with results from τ decay. The important ingredient for this consistent understanding is the existence of a strong nonpole background $T_{\rm np}$ contributing to the total $\pi\rho$ amplitude T. This background does *not* appear explicitly in τ decay. It can be shown [17] that the coupling of the W boson to the $\pi\rho$ system may be written as

$$f_{W\to\pi\rho} = f^{(0)}_{W\to\pi\rho} + f^{(0)}_{W\to\pi\rho} D T_{\rm np} + f^{(0)}_{W\to A_1} \tilde{d} f_{A_1\to\pi\rho} \tag{39}$$

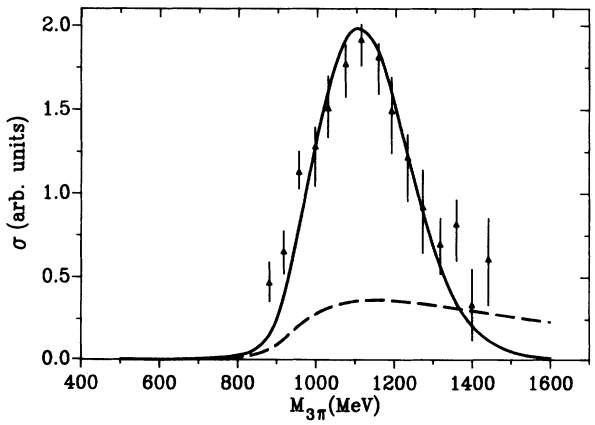

FIG. 13. The A_1-mass spectrum for our full model (solid line). The pole is fixed at $1260 - i\,400/2$ MeV. The dashed line shows the nonpole part of the mass spectrum which is included in the full calculation.

[f: total (dressed) vertex function, $f^{(0)}$: bare vertex function]. But in the framework of axial vector dominance the direct coupling $f^{(0)}_{W\to\pi\rho}$ and therefore the contribution including $T_{\rm np}$ explicitly vanishes. For the charge-exchange reaction, on the other hand, the full $\pi\rho$ T matrix contributes and the strong nonpole background (dashed curve in Fig. 13) allows the connection of A_1 parameters and mass spectrum. Finally we would like to note that π exchange which was included in some investigations of diffractive production [16] is (at least in our model) not sufficient to generate a nonpole background strong enough to remove the discrepancy. It is the ρ exchange that is responsible for the bulk contribution to $T_{\rm np}$. We complete the discussion of the axial vector partial wave with Fig. 14 showing the t dependence of the A_1 mass spectrum. Besides the result of our full model A for $t=0$ it gives the mass spectrum for $t=-(0.45\ \text{GeV})^2$, a value which is given in [15] as the upper bound of the momentum transfer in the experiment. The t dependence is quite small justifying our previous approximation to calculate the mass spectrum only for $t=0$.

Having obtained a good description of the A_1 channel we now turn to the ω partial wave. The parameters for the nonpole part are fixed now; the bare mass $m^{(0)}_\omega$ and the bare coupling constant $g^{(0)}_{\omega\pi\rho}$ are chosen to generate a pole at $m_\omega - i\Gamma_\omega/2$. The only remaining parameter is the cutoff mass Λ appearing in the $\omega\to\pi\rho$ vertex function [Eq. (27)]. Table II shows the complete set of parameters we use in this calculation. $g^{(0)}_{\omega\pi\rho}$ is rather large, it is about a factor of 8 larger than the physical one. This large value for $g^{(0)}$ is necessary to reproduce the small width of the ω meson. Figure 15 shows the resulting mass spectrum in comparison with experimental data from [15]. The normalization is of course the same as in Fig. 13. We get a good qualitative description of the empirical situation for the pole region as well as for the high energy tail. It is interesting to note that no shift between ω mass and maximum of the bump is observed, in contrast to the A_1 channel and in agreement with experimental data. The mass of the ω meson lies about 130 MeV below $\pi\rho$ threshold; the nonpole amplitude of $\pi\rho$ scattering is due to phase-space quite small in this region and therefore no effect on the ω mass spectrum can be observed. The situation is different in the axial vector channel where the mass of the A_1 meson and the important part of the nonpole amplitude coincide.

TABLE II. Parameters of our model A [for pole diagrams $(g^{(0)})^2/4\pi$ is given].

Diagram	$g^2/4\pi$	$m^{(0)}$ (MeV)	Λ (MeV)	Form factor
π exchange	2.84	-	800	monopole
ρ exchange	2.84	-	1350	monopole
A_1 pole	1.237	1288	2600	dipole
ω pole	52.170	1144	1300	dipole

Finally we will look at the π channel. This partial wave is of special importance for us since our main motivation to investigate $\pi\rho$ scattering has been our plan to apply it to the πNN form factor and to correlated $\pi\rho$ exchange in the NN interaction. In both cases it is the π partial wave where open questions may be answered when $\pi\rho$ scattering is included. Unfortunately, no data are given for this partial wave in [15]. However, we are confident that our results are reliable since we have checked our interaction model in the A_1- and ω-partial waves, and all parameters are fixed now. Figure 16 shows the mass spectrum in the π channel (solid line). To get a feeling for its strength we have also plotted the nonpole mass spectrum of the A_1 channel for comparison (dashed line). The nonpole amplitude was important in the axial channel and Fig. 16 demonstrates that it is of equally strong magnitude in the π channel.

We have shown that our three-body model A provides a good description in all channels of physical interest. Although we already found results which are interesting by themselves (analysis of A_1) it was our main aim to evaluate a realistic $\pi\rho$ interaction model to apply it to several processes of medium energy physics. This is somewhat difficult with model A since in this framework we cannot calculate the full off-shell T matrix which is needed for the applications. Besides simplicity reasons this was the main motivation for us to develop a second model for

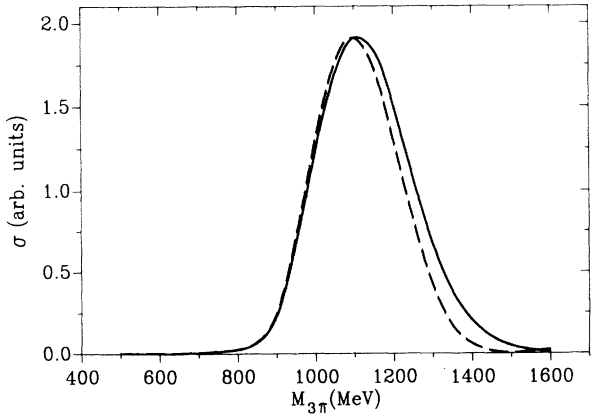

FIG. 14. t dependence of the mass spectrum. The solid line shows the result of our full model, i.e., $t=0$. The dashed line shows the mass spectrum for $t=-(0.45\ \text{GeV})^2$, cf. Ref. [15].

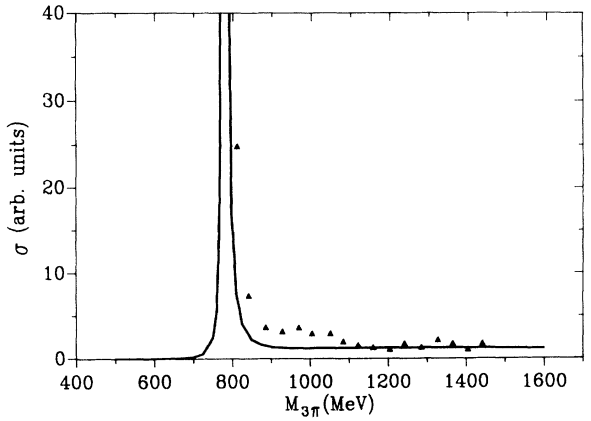

FIG. 15. The mass spectrum in the ω channel. Data are from Ref. [15] and normalization is as in Fig. 13.

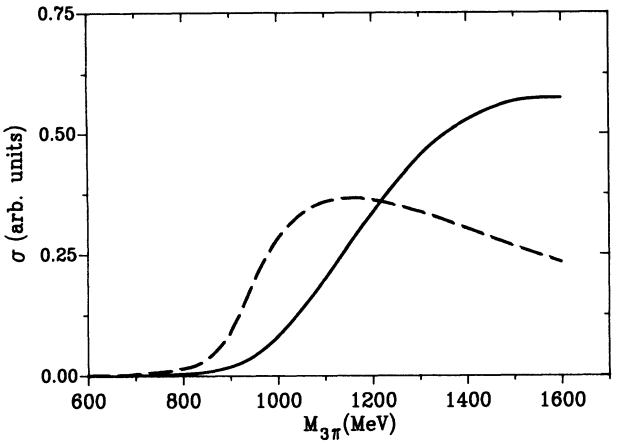

FIG. 16. The mass spectrum in the π channel (solid line). Normalization as in Fig. 13. The dashed line shows the nonpole mass spectrum of the A_1 channel for comparison.

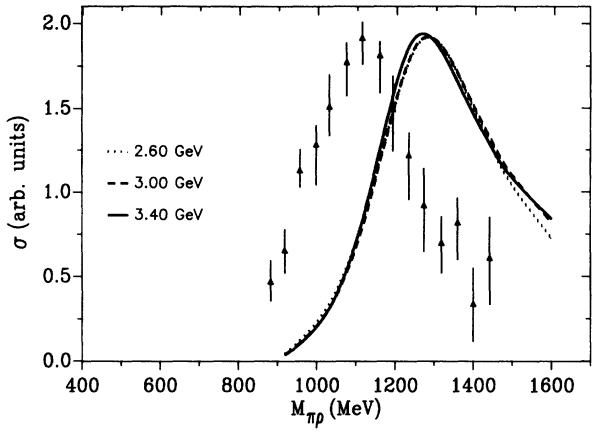

FIG. 17. The A_1-mass spectrum using model B and including only the A_1-pole diagram. The different curves are obtained for different values of the cutoff mass appearing in the $A_1 \to \pi\rho$ vertex function.

$\pi\rho$ scattering in which the ρ is considered to be a stable particle (model B). We will demonstrate now that our model B has all the important features that have been shown to be crucial for the description of the empirical situation when we discussed model A. Having tested the reliability of the simple model it can then be used in the desired applications.

Besides the approximations already made in the calculation of the $\pi\rho$ T matrix in model B additional assumptions are necessary to calculate the mass spectrum. If the incoming pion is on mass shell the incoming ρ is also on mass shell, i.e., $t = k_\rho^2 = m_\rho^2 > 0$. The off-shell structure of model B does therefore not allow the calculation of the T matrix in the correct region of q_π and k_ρ. However, we assume that the t dependence is rather small and that the conclusions concerning the *shape* of the mass spectrum are not affected if we use the on-shell T matrix to calculate the mass spectrum, which is then defined by

$$\sigma \equiv \sigma_{\pi\rho}(t=m_\rho^2, M_{\pi\rho}) = \int d\Omega_2 \, T_{\pi\rho} T_{\pi\rho}^\dagger \, . \qquad (40)$$

As for model A we start our discussion in the A_1 channel and investigate the relation between the A_1 pole and the shape of the mass spectrum. Figure 17 shows the model B calculation corresponding to Fig. 11. The pole is again fixed at $1260 - i\,200$ MeV to reproduce the A_1 parameters and we calculate the mass spectrum without the inclusion of any exchange diagram. It is obvious that the use of model B does not change our previous conclusion, namely that it is impossible to get a good description of the mass spectrum. Fortunately also our solution to this problem remains valid for model B. Figure 18 shows the resulting mass spectrum when the nonpole part of the potential is switched on. We get a comparably good description of the data; the main difference lies in the fact that the mass spectrum falls off very rapidly at $\pi\rho$ threshold now. The nonpole part must be sufficiently strong to reproduce the mass spectrum and this requirement again fixes the cutoff masses for π and ρ exchange.

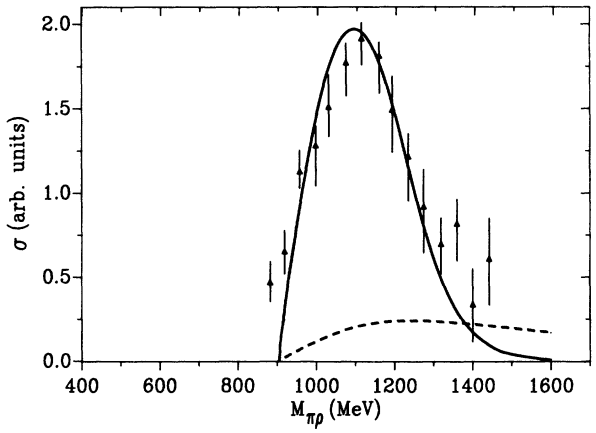

FIG. 18. The A_1-mass spectrum for our full model B. The dashed line shows the nonpole mass spectrum for comparison.

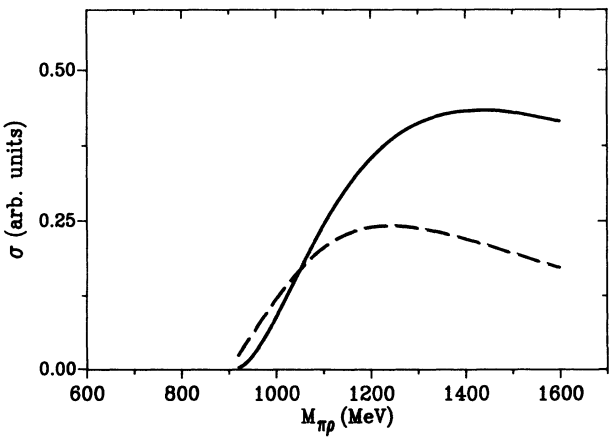

FIG. 19. The mass spectrum in the π channel using model B (solid line). Normalization as in Fig. 18. The dashed line shows the nonpole mass spectrum of the A_1 channel for comparison.

TABLE III. Parameters of our model B [for pole diagrams $(g^{(0)})^2/4\pi$ is given].

Diagram	$g^2/4\pi$	$m^{(0)}$ (MeV)	Λ (MeV)	Form factor
π exchange	2.84	-	800	monopole
ρ exchange	2.84	-	1350	monopole
A_1 pole	1.221	1232	3200	dipole
ω pole	4.853	801	1000	dipole

All parameters of model B are given in Table III.

The situation turns out to be more difficult in the ω channel. In model B the bump with a width of 8 MeV, see Fig. 15, is replaced by a delta function indicating a zero-width ω meson. Our model B cannot describe the magnitude of the high energy tail of the ω as in model A. Below $\pi\rho$ threshold the mass spectrum is clearly zero but also for higher energies our result is too small compared to the data. The high energy tail in Fig. 15 is due to the correct description of the ω-pole diagram in model A. The treatment of model B just ensures that we get a pole at the ω mass with the right residue but we cannot expect that this approximation provides an overall description of the data which is as well as it was for model A. However, the disagreement in the ω channel does not affect the reliability of the nonpole part of the T matrix. It is a problem of principle that model B can generate only a zero-width ω meson but this difficulty is not caused by the nonpole part which has been proven to be realistic in the A_1 channel.

In the π channel where we want to apply the $\pi\rho$ interaction no pole diagrams close to threshold interfere with the nonpole part. Figure 19 shows the nonpole mass spectra for the A_1 and π channel. As in model A the $\pi\rho$ interaction is about equally strong for the π channel as for the A_1 channel and for the latter it was shown to be quite important. This can also be seen from the potential (Fig. 8): Its magnitude is comparable in all three channels of physical interest. It is this strong nonpole amplitude in the π partial wave that encourages us to investigate the πNN form factor and correlated $\pi\rho$ exchange where this part of the $\pi\rho$ interaction enters.

IV. SUMMARY AND OUTLOOK

In this paper, we have developed a dynamical model for $\pi\rho$ scattering. The starting point was a pseudopotential based on s- as well as t-channel meson exchange. We first investigated the more realistic case of a broad ρ meson and applied the relativistic three-body theory of Aaron, Amado, and Young [7] to $\pi\rho$ scattering. The results have been compared with data from charge-exchange reactions and good agreement was obtained in all relevant channels. Especially in the axial vector partial wave the strong nonpole background which is generated mainly by ρ exchange turned out to be crucial for a consistent understanding of the A_1 meson.

However, although our three-body model produces good agreement with experimental data, it cannot be used to calculate a fully off-shell T matrix, which is required in most applications of $\pi\rho$ scattering. We therefore developed, in addition to the rather complicated instable ρ model, a simpler model assuming the ρ to be a stable particle. The previous results have been used to test this simple model and it was shown that the main conclusions do not change.

It turned out that the nonpole amplitude is comparably strong in P waves (π, ω channel) as in the S wave (A_1 channel) where it was responsible for the consistent description of the A_1 meson. To underline the importance of $\pi\rho$ scattering in the pionic channel we have recently calculated the πNN form factor in a meson-exchange framework including the simple model for $\pi\rho$ scattering [5]. It turned out that this interaction has indeed a large effect leading to an appreciable softening of the form factor. The final result is rather soft ($\Lambda_{\pi NN} \simeq 1$ GeV) in agreement with information from other sources [4].

The next step must be the inclusion of such a soft form factor in the Bonn potential of the NN interaction [2]. It is again the strong nonpole contribution in the pionic channel of the $\pi\rho$ interaction that encourages us to regard correlated $\pi\rho$ exchange as a possible solution for the problems arising from a soft πNN form factor. We are confident that this process generates additional tensor force in the NN interaction, which one needs if a soft πNN vertex is used. Calculations along this line are in progress.

ACKNOWLEDGMENTS

The authors would like to thank B. C. Pearce for many useful discussions. His assistance was essential for the solution of many problems especially concerning the treatment of pole diagrams. Thanks are also due to J. W. Durso for numerous stimulating discussions and continuous interactions. This work was supported in part by the Science & Technology Cooperation Germany/Canada (KAN-BSC 13).

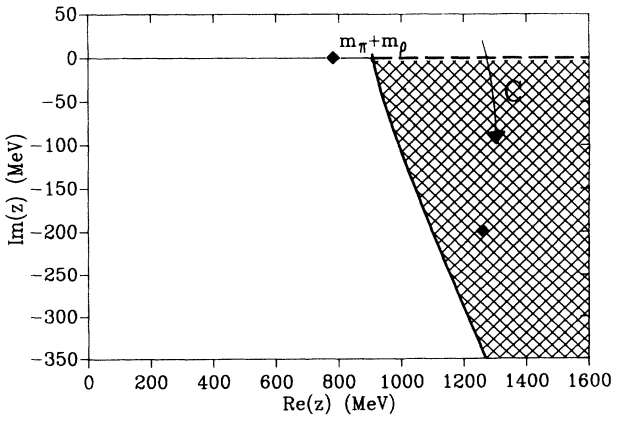

FIG. 20. The cut structure of the two-body propagator G. The squares mark the ω and A_1 pole, $z = \sqrt{s}$. The dashed line shows the cut for real momenta, the solid one for a momentum contour rotated by an angle of $\Theta = 31°$. The shaded area shows the region of the second sheet we can explore with this contour.

APPENDIX: DETERMINATION OF POLES

The self-energy $\Sigma = f^{(0)}Gf$ or $\Sigma = f^{(0)}Df$ contains the intermediate propagator G or D and reflects the multisheet structure of the scattering amplitude. To find the poles of the T matrix one has to investigate the cut structure of these propagators [18]

$$G(s,p) \sim [\sqrt{s} - \omega_\pi(p) - \omega_\rho(p) + i\epsilon]^{-1} . \quad \text{(A1)}$$

For a momentum contour along the real axis G has a cut along the real axis of the complex $\sqrt{s}$ plane starting at $\sqrt{s} = m_\pi + m_\rho$ (Fig. 20). If we want to calculate $\Sigma(s)$ for values of $\sqrt{s}$ in the lower complex half plane (e.g., $\sqrt{s}$ moving along path C in Fig. 20), we have to avoid crossing this cut. This can be achieved by rotating the momentum contour by an angle Θ into the lower half plane. This procedure effectively rotates the cut into the complex $\sqrt{s}$ plane and the new position is given by

$$\sqrt{s} - \omega_\pi(pe^{-i\Theta}) - \omega_\rho(pe^{-i\Theta}) = 0 . \quad \text{(A2)}$$

The result is shown in Fig. 20. We are now able to calculate $\Sigma(s)$ for values of $\sqrt{s}$ in the dotted area, i.e., we can investigate $\Sigma(s)$ on the second energy sheet since it is now continuous along path C in Fig. 20.

In the three-body case Σ contains the more complicated propagator D given by Eq. (14) which obtains two cuts. One is generated by the 2π self-energy appearing in the denominator of D and is given by

$$\sigma_p - 4\omega_{p'}^2 = 0 . \quad \text{(A3)}$$

For real p and a p' contour following the real axis this equation defines a cut along the real $\sqrt{s}$ axis starting at $\sqrt{s} = 3m_\pi$ [Fig. 21(a)]. The second cut is generated by the two-body resonance in the three-body system and is defined by

$$\sigma_p = (m_\rho - i\Gamma_\rho/2)^2 . \quad \text{(A4)}$$

This cut lies in the complex plane and has a branch point at $(m_\pi + m_\rho, -\Gamma_\rho/2)$. To explore the regions of the complex plane where the ω and A_1 poles are located we have to rotate both, p and p' contour, into the lower complex half plane. Figures 21(b,c) show the resulting rotation of the cuts in the $\sqrt{s}$ plane. In Fig. 21(b) $\Theta = 12°$ and we are able to look for an A_1 pole on the second sheet. In Fig. 21(c) we have chosen $\Theta = 31°$ exploring the third energy sheet.

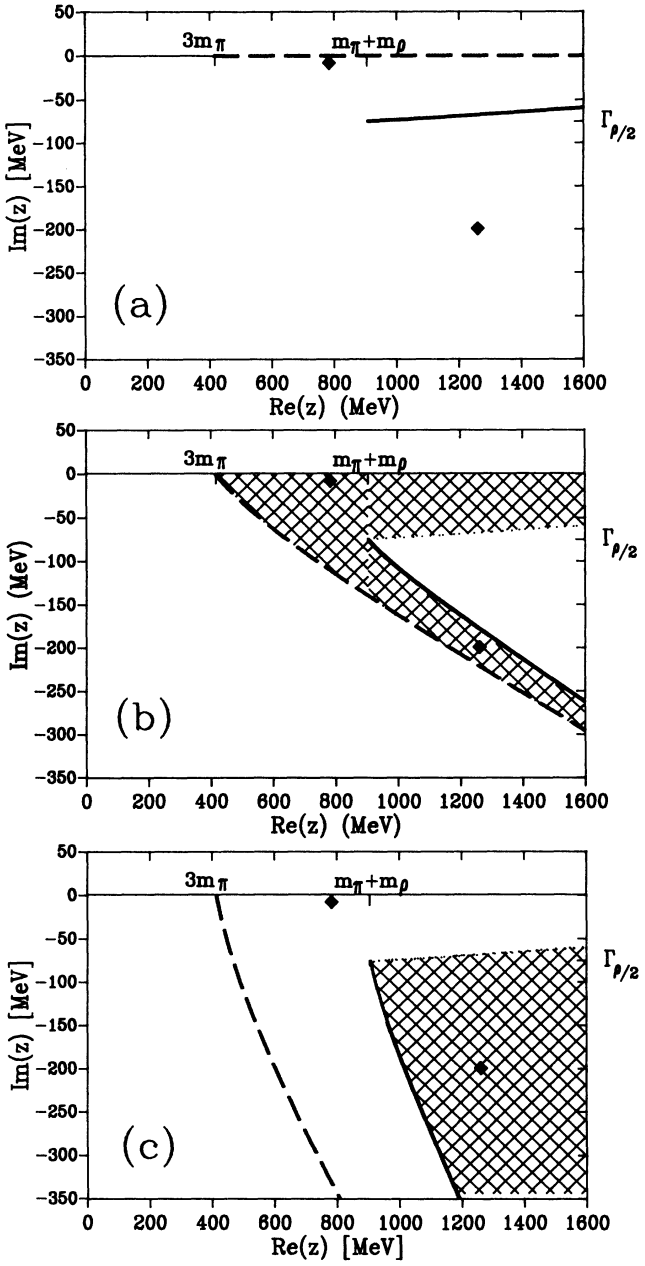

FIG. 21. (a) The cut structure of the three-body propagator D for real momenta. Notation as in Fig. 18. (b) The same for both momentum contours (p and p') rotated by an angle of $\Theta = 12°$. The shaded area shows the region of the second sheet we can explore. (c) Both momentum contours rotated by an angle of $\Theta = 31°$. The shaded area shows the region of the third sheet we can investigate.

[1] G. E. Brown and A. D. Jackson, *The Nucleon-Nucleon Interaction* (North-Holland, Amsterdam, 1979); M. Lacombe, B. Loiseau, J. M. Richard, R. Vinh Mau, J. Côté, P. Pirès, and R. de Tourreil, Phys. Rev. C **21**, 861 (1980); M. M. Nagels, T. A. Rijken, and J. D. de Swart, Phys. Rev. D **17**, 768 (1978).

[2] R. Machleidt, K. Holinde, and Ch. Elster, Phys. Rep. **149**, 1 (1987).

[3] D. Lohse, J. W. Durso, K. Holinde, and J. Speth, Nucl. Phys. **A516**, 513 (1990).

[4] S. A. Coon and M. D. Scadron, Phys. Rev. C **23**, 1150 (1981); Phys. Rev. C **42**, 2256 (1990); A. W. Thomas and K. Holinde, Phys. Rev. Lett. **63**, 2025 (1989).

[5] G. Janssen, J. W. Durso, K. Holinde, B. C. Pearce, and J. Speth, Phys. Rev. Lett. **71**, 1978 (1993).

[6] L. D. Faddeev, *Mathematical Aspects of the Three-Body Problem* (Davey, New York, 1965).

[7] R. Aaron, *Modern Three-Hadron Physics*, edited by

A. W. Thomas (Springer-Verlag, Heidelberg, 1976); R. Aaron, R. D. Amado, and J. E. Young, Phys. Rev. **174**, 2022 (1968).
[8] R. K. Bhaduri, *Models of the Nucleon* (Addison-Wesley, Reading, MA, 1988).
[9] M. Bando, T. Kugo, and K. Yamawaki, Phys. Rep. **164**, 217 (1988).
[10] J. W. Durso, Phys. Lett. B **184**, 348 (1987).
[11] R. Blankenbecler and R. Sugar, Phys. Rev. **142**, 1051 (1966).
[12] B. C. Pearce and I. R. Afnan, Phys. Rev. C **34**, 991 (1986); I. R. Afnan and A. T. Stelbovics, Phys. Rev. C **23**, 1384 (1981).
[13] Particle Data Group, K. Hikasa *et al.*, Phys. Rev. D **45**, 100 (1992).
[14] M. G. Bowler, Phys. Lett. B **182**, 400 (1986).
[15] J. A. Dankowych *et al.*, Phys. Rev. Lett. **38**, 580 (1981).
[16] R. Aaron, R. S. Longacre, and J. E. Sacco, Ann. Phys. (N.Y.) **117**, 56 (1979); R. S. Longacre and R. Aaron, Phys. Rev. Lett. **38**, 1509 (1977).
[17] B. C. Pearce (private communication).
[18] B. C. Pearce and I. R. Afnan, Phys. Rev. C **30**, 2022 (1984).